



Dynamic localization of a helper NLR at the plant–pathogen interface underpins pathogen recognition

Cian Duggan^a, Eleonora Moratto^a, Zachary Savage^a, Eranthika Hamilton^a, Hiroaki Adachi^{b,c}, Chih-Hang Wu^{b,d}, Alexandre Y. Leary^a, Yasin Tuntas^a, Stephen M. Rothery^a, Abbas Maqbool^b, Seda Nohut^a, Toby Ross Martin^a, Sophien Kamoun^b, and Tolga Osman Bozkurt^{a,1}

^aDepartment of Life Sciences, Imperial College, SW7 2AZ London, United Kingdom; ^bThe Sainsbury Laboratory, University of East Anglia, NR4 7UH Norwich, United Kingdom; ^cGraduate School of Biological Sciences, Nara Institute of Science and Technology, Ikoma 630-0192, Japan; and ^dInstitute of Plant and Microbial Biology, Academia Sinica, Taipei 11529, Taiwan

Edited by David C. Baulcombe, University of Cambridge, Cambridge, United Kingdom, and approved June 29, 2021 (received for review March 17, 2021)

Plants employ sensor–helper pairs of NLR immune receptors to recognize pathogen effectors and activate immune responses. Yet, the subcellular localization of NLRs pre- and postactivation during pathogen infection remains poorly understood. Here, we show that NRC4, from the “NRC” solanaceous helper NLR family, undergoes dynamic changes in subcellular localization by shuttling to and from the plant–pathogen haustorium interface established during infection by the Irish potato famine pathogen *Phytophthora infestans*. Specifically, prior to activation, NRC4 accumulates at the extrahaustorial membrane (EHM), presumably to mediate response to periahaustorial effectors that are recognized by NRC4-dependent sensor NLRs. However, not all NLRs accumulate at the EHM, as the closely related helper NRC2 and the distantly related ZAR1 did not accumulate at the EHM. NRC4 required an intact N-terminal coiled-coil domain to accumulate at the EHM, whereas the functionally conserved MADA motif implicated in cell death activation and membrane insertion was dispensable for this process. Strikingly, a constitutively autoactive NRC4 mutant did not accumulate at the EHM and showed punctate distribution that mainly associated with the plasma membrane, suggesting that postactivation, NRC4 may undergo a conformation switch to form clusters that do not preferentially associate with the EHM. When NRC4 is activated by a sensor NLR during infection, however, NRC4 forms puncta mainly at the EHM and, to a lesser extent, at the plasma membrane. We conclude that following activation at the EHM, NRC4 may spread to other cellular membranes from its primary site of activation to trigger immune responses.

helper NLR | plant disease resistance | host–microbe interactions | cell biology

Filamentous pathogens cause devastating diseases on crops, posing a major threat to food security. Some oomycete and fungal pathogens produce specialized hyphal extensions called haustoria that invade the host cells. Haustoria are critical infection structures implicated in delivery of effector proteins and nutrient uptake (1–6). These specialized infection structures are accommodated within the plant cells but are excluded from the host cytoplasm through a newly synthesized membrane called the extrahaustorial membrane (EHM). An intriguing, yet poorly understood, observation is that the EHM is continuous with the host plasma membrane (PM) but is distinct in lipid and protein composition (7, 8). Most of the proteins embedded in the PM, such as surface immune receptors, are excluded from the EHM (9–11). Despite its critical role as the ultimate interface mediating macromolecule exchange between the host and parasite, the mechanisms underlying the biogenesis and functions of the EHM are poorly understood (12).

Pathogens deliver effector proteins inside the host cells to neutralize immune responses and enable parasitic infection. A well-studied class of effectors delivered via haustoria are the RXLR family of effectors secreted by *Phytophthora infestans*

(2, 6, 13). RXLR effectors traffic to diverse plant cell compartments to suppress host immunity and mediate nutrient uptake. Remarkably, several *P. infestans* RXLR effectors focally accumulate at the haustorium interface and perturb cellular defenses (7, 13–15). These include AVRblb2 and AVR1, both of which are implicated in targeting host defense-related secretory pathways to contribute to pathogen virulence (14, 16). Notably, all *P. infestans* isolates harbor multiple *Avrblb2* paralogues (17), which are recognized by the broad-spectrum disease resistance gene *Rpi-blb2* cloned from the wild potato species *Solanum bulbocastanum* (14, 18, 19). On the other hand, AVR1 is sensed by the late blight resistance gene *RI*, which provides race-specific resistance to AVR1 carrying *P. infestans* strains (20).

Both *Rpi-blb2* and *RI* encode nucleotide-binding (NB), leucine-rich repeat (LRR) (NLR) proteins, which belong to an NLR network in solanaceae and other asterid plants known as the NLR REQUIRED FOR CELL DEATH (NRC) family. The NRC immune network members form a superclade that consists of about one-third of all Solanaceae NLRs, providing disease resistance to nematodes, viruses, bacteria, oomycetes, and aphids (21).

Significance

Plant NLRs function as intracellular immune sensors of pathogen virulence factors known as effectors. In the resting state, NLRs localize to subcellular sites where the effectors they sense operate. However, the extent to which NLRs alter their subcellular distribution during infection remains elusive. We describe dynamic changes in spatiotemporal localization of an NLR protein in infected plant cells. Specifically, the NLR protein accumulates at the newly synthesized plant–pathogen interface membrane, where the corresponding effectors are deployed. Following immune recognition, the activated receptor reorganizes to form punctate structures that target the cell periphery. We propose that NLRs are not necessarily stationary receptors but instead may spread to other cellular membranes from the primary site of activation to boost immune responses.

Author contributions: C.D., E.M., Z.S., H.A., C.-H.W., S.K., and T.O.B. designed research; C.D., E.M., Z.S., E.H., H.A., C.-H.W., A.Y.L., Y.T., S.N., T.R.M., and T.O.B. performed research; C.D., E.M., Z.S., E.H., H.A., C.-H.W., A.Y.L., Y.T., S.M.R., A.M., S.N., T.R.M., S.K., and T.O.B. contributed new reagents/analytic tools; C.D., E.M., Z.S., E.H., S.K., and T.O.B. analyzed data; C.D., E.M., Z.S., E.H., H.A., Y.T., A.M., T.R.M., S.K., and T.O.B. edited the manuscript; and C.D. and T.O.B. wrote the paper.

Competing interest statement: S.K. receives funding from industry on NLR biology.

This article is a PNAS Direct Submission.

Published under the PNAS license.

¹To whom correspondence may be addressed. Email: o.bozkurt@imperial.ac.uk.

This article contains supporting information online at <https://www.pnas.org/lookup/suppl/doi:10.1073/pnas.2104997118/-DCSupplemental>.

Published August 20, 2021.

Within the NRC network, sensor NLRs specialized to recognize effectors secreted by pathogens are coupled to helper NLRs (NRCs) that translate the defense signal into disease resistance. We recently showed that Rpi-blb2 and R1 are “sensor NLRs” that require the “helper NLR” NRC4 for the immune-related programmed cell death known as the hypersensitive response (HR) and subsequent disease resistance (21). How and where AVRblb2 and AVR1 are recognized by the NRC4 helper–sensor pairs, as well as the mechanism that leads to HR and disease resistance following their recognition, is unknown. Because AVRblb2 and AVR1 localize to the EHM (13, 14), it is likely that the NLR receptor pairs that sense these periaustorial effectors also accumulate at the haustorial interface. So far, live-cell imaging of NLRs during infection, which would allow for a greater understanding of NLR functions, has not been feasible due to cell death activation. However, recently solved structures of activated NLRs uncovered critical residues that can be mutated to avoid HR activation without perturbing other NLR functions such as effector recognition and self-oligomerization following activation (22–24). Therefore, fluorescent protein fusions of these NLR mutants could be used for cell biology studies to investigate NLR activities during infection.

All NLRs in the NRC superclade carry N-terminal coiled-coil (CC) domains, a characteristic of the CC-NLR type of immune receptors. The recently resolved cryogenic electron microscopy (cryo-EM) structures of activated/nonactivated forms of the CC-NLR type of resistance protein AtZAR1 (22, 25), which provides resistance to several bacterial species, revealed an intriguing model for HR elicitation. Upon activation, AtZAR1 (hereafter, ZAR1) oligomerizes into an inflammasome-like structure, called a “resistosome.” The ZAR1 resistosome consists of five ZAR1 proteins that assemble into a pentameric structure together with the kinases required for ZAR1 activation. Intriguingly, upon immune activation, the first alpha helix ($\alpha 1$) within the CC domain of ZAR1 is exposed and the five $\alpha 1$ helices of the ZAR1 pentamer assemble into a funnel-shaped structure. The resistosome inserts into the PM, forming a pore that could disrupt the cellular integrity or lead to ion flux across the membrane leading to an HR (26, 27). This challenged the long-held view that NLRs execute HR and resistance through activation of downstream signaling cascades. However, whether this model could be applied to other NLRs is still unknown.

We recently made an exciting discovery that an N-terminal motif (“the MADA motif”) overlapping ZAR1’s $\alpha 1$ helix, with the consensus sequence MADAxVSFxVxKLxxLLxxEx, exists in ~20% of CC-NLRs from monocot and dicot species. Remarkably, this motif is preserved in NRC helpers but not in their sensor mates (23). Intriguingly, the first 29 amino acids (aa) of NRC4 containing the MADA motif elicited HR when fused to YFP on its C terminus but not when it is tagged with the YFP mutant that cannot oligomerize. These results indicated that the N terminus of NRC4 relies on a scaffold such as YFP or the rest of NRC4 to form oligomers and trigger cell death. Notably, we previously showed that a chimeric NRC4 construct carrying ZAR1’s $\alpha 1$ helix is functional for triggering HR and confers disease resistance when coexpressed with Rpi-blb2 in lines lacking NRC4 (23), indicating that the proposed ZAR1 mode of action could be applied to NRC helpers.

Although recent structural studies greatly improved our understanding of the NLR-mediated immunity and provide unprecedented insights into NLR mode of action, subcellular distribution of NLRs during infection with relevant pathogens is unknown. In the absence of infection, NLRs have been shown to localize to various cellular compartments such as cytoplasm, PM, nucleus, and tonoplast (28–32). These compartments can be required for effector recognition, subsequent HR activation, and/or immune signaling, and some NLRs require a shift in their localization to perceive the effector and initiate the immune responses (30, 32–36). However, determining the subcellular localization of NLRs during infection by relevant microbes has not been feasible due to activation of HR

when the corresponding effector is present. Nevertheless, it is possible to monitor the distribution of the NRC helpers in plants that lack the sensor NLRs specialized to recognize the pathogen. The solanaceous model plant *Nicotiana benthamiana* is an excellent system to study the functioning of the Rpi-blb2-NRC4 pair as it contains a functional NRC4 but lacks specialized sensor NLRs that can recognize *P. infestans*, whereas transgenic plants carrying Rpi-blb2 are fully resistant to *P. infestans* (14, 18, 19).

Here, we describe the dynamic changes in spatiotemporal localization of NRC4 in response to infection by *P. infestans*. NRC4 accumulates at the newly synthesized EHM, where the corresponding effectors AVRblb2 and AVR1 are deployed (13, 14). Following immune recognition, the activated receptor reorganizes to form punctate structures that target the cell periphery. Our results indicate that NLRs are not necessarily stationary immune receptors but instead can alter their localizations during infection and may further spread to other cellular membranes from the primary site of activation to boost immune responses.

Results

Unlike NRC2 and ZAR1, Nonactivated NRC4 Accumulates at the EHM during *P. infestans* Infection. It has not been possible to investigate NLR subcellular localization during infection with relevant microbes due to HR cell death. However, it is feasible to monitor helper NLRs during infection in the absence of sensor NLRs. The *N. benthamiana*–*P. infestans* pathosystem offers excellent tools to investigate helper NLR functions because *N. benthamiana* lacks sensor NLRs that can prevent infection by *P. infestans*. *N. benthamiana* contains two alleles of NRC4 helper (NRC4a/b), which can pair with either of the sensor NLRs Rpi-blb2 or R1 to recognize *P. infestans* effector protein AVRblb2 and R1 (14, 18, 19, 21, 23). Since both AVRblb2 and AVR1 accumulate at the haustorium interface (7, 13, 14), we reasoned that the corresponding sensor–helper pairs may be positioned at the EHM to detect these effectors.

Unfortunately, the sensor NLRs Rpi-blb2 and R1 produced too low fluorescence to accurately monitor during infection and caused cell death under endogenous conditions—that is, when NRC4 was present. Thus, we decided to investigate the localization of fluorescently tagged helper NRC4 in *N. benthamiana* during *P. infestans* infection. Strikingly, consistent with the localization pattern of the periaustorial AVR effectors, both N- and C-terminal fusions of NRC4 accumulated around the haustorium when transiently expressed (Fig. 1A and B). GFP fusions of NRC4 produced bright fluorescent signal around the haustorium but not throughout the cell, whereas in uninfected cells NRC4 showed mainly a cytoplasmic distribution much like the GFP control, except that NRC4 was excluded from the nucleus (Fig. 1C and E–H). We then confirmed accumulation of NRC4 around the haustorium by live-cell imaging during infection of stable transgenic *NRC4-GFP N. benthamiana* lines with red fluorescent tdTomato *P. infestans* (Fig. 1D). To further illustrate that NRC4’s periaustorial accumulation pattern is not an optical artifact, we next coexpressed NRC4 C-terminally fused to orange fluorescent tag mKOk with GFP control and performed live-cell imaging during infection. In agreement with the results obtained when NRC4-GFP was expressed alone (Fig. 1A), NRC4-mKOk produced a sharp fluorescence signal around the haustorium, unlike GFP control, which displayed a uniform distribution pattern throughout the cell (Fig. 1I and Movie S1). These results strongly suggest that NRC4 shifts its localization from cytosol to haustorium interface during infection.

In many cases, fluorescent fusions of NLRs lead to inactivity. Therefore, we next determined whether GFP fusions of NRC4 are functional. To do this, we generated CRISPR/Cas9 mutants of NRC4a/b in the Rpi-blb2 transgenic background (hereafter, Rpi-blb2^{NRC4a/b}) and employed an HR complementation assay where the ability of NRC4 to trigger HR cell death in the absence of *P. infestans* was assayed by coexpressing AVRblb2 with

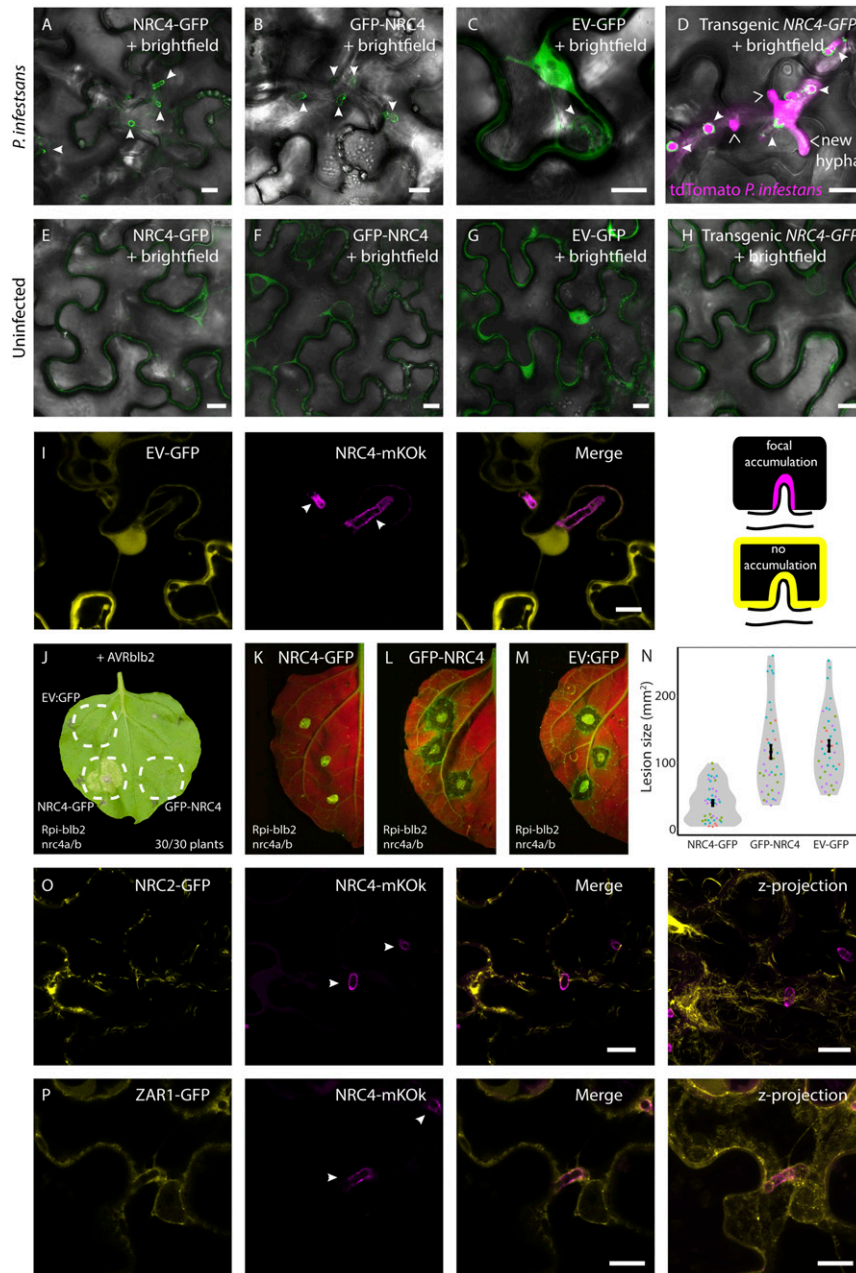


Fig. 1. NRC4, but not NRC2 or ZAR1, accumulates at the EHM. (A–C) Single-plane confocal micrographs showing transient expression of NRC4-GFP and GFP-NRC4 but not EV-GFP accumulates around *P. infestans* haustoria (arrowheads). (D) Transgenic NRC4-GFP focally accumulates around red fluorescent tdTomato *P. infestans* haustoria. Open arrowheads indicate the newly forming hyphae between cells. (E–G) Transient expression of NRC4-GFP, GFP-NRC4, and EV-GFP all localize to the cytoplasm in uninfected cells. (H) Transgenic NRC4-GFP is also cytoplasmic in uninfected cells. (I) Single-plane images transiently expressing EV-GFP with NRC4-mKOK during infection with *P. infestans* showing EV-GFP does not focally accumulate around haustoria but localizes to the cytoplasm throughout the cell, including around haustoria, whereas NRC4-mKOK accumulates around haustoria. Cartoons (Right) describe this result further. (J) NRC4-GFP but not GFP-NRC4 or EV-GFP genetically complement CRISPR/Cas9 mutation of NRC4a/b in Rpi-blb2 transgenic background by triggering HR when coexpressed with AVRblb2. The result was replicated in 30 plants over three independent experiments. Images were taken at 8 d post agroinfiltration (dpi). (K–N) NRC4-GFP but not GFP-NRC4 or EV-GFP provides resistance to *P. infestans*. We expressed NRC4 fusions or EV-GFP on a leaf opposite one another, and after 1 d infected the leaves with *P. infestans*. At 8 d postinfection (dpi), the area (mm²) of the necrotic lesions was measured on white light images, and the average of three infection spots was plotted as points on the scatter violin plot (N), where each construct had $n > 37$ plants/leaves over four independent experimental replicates. The mean and SE are shown as points and bars, respectively. Unpaired Wilcoxon tests gave P values of 1.26×10^{-9} for NRC4-GFP to GFP-NRC4, 7.13×10^{-12} for NRC4-GFP to EV-GFP, and 0.25 for GFP-NRC4 to EV-GFP. (O and P) Transient expression of NRC2-GFP or ZAR1-GFP shows they do not accumulate around haustoria unlike NRC4-mKOK, which focally accumulates. First three images are single plane, last images are z-projections of 10 or 11 z-slices, respectively. (O) NRC2 localizes to disperse filaments. (P) ZAR1 localizes diffusely in the cytoplasm. (Scale bars, 10 μ m.)

GFP fusions of NRC4 or an empty vector (EV)-GFP control in mutant plants. Infiltrated leaf patches on Rpi-blb2^{nrc4a/b} plants rescued the cell death phenotype by producing clear HR symptoms with C-terminally tagged NRC4 (NRC4-GFP) ($n = 30$ plants, 100%) but not with EV-GFP ($n = 30$ plants, 0%) or N-terminally tagged NRC4 (GFP-NRC4) ($n = 30$ plants, 0%) (Fig. 1J), showing that only the C-terminal GFP fusion is functional. This was not due to reduced stability of GFP-NRC4 as Western blotting of this construct produced a stronger protein band compared to NRC4-GFP (SI Appendix, Fig. S1). We further validated that NRC4-GFP but not GFP-NRC4 or EV-GFP could genetically complement Rpi-blb2^{nrc4a/b} plants and rescue resistance to *P. infestans* (Fig. 1K–N). These results are consistent with the finding that an N-terminal tag on ZAR1 inhibits its cell death function (37), possibly by blocking the $\alpha 1$ helix insertion into the membrane.

To determine if other NLRs can also accumulate around haustoria, or if this phenomenon is specific to NRC4, we investigated the localization of two other MADA motif-containing NLRs NRC2 and ZAR1. NRC2, like NRC4, recognizes a range of effectors from *P. infestans*, viruses, nematodes, bacteria, and insects, via sensor NLRs (21). ZAR1 recognizes a range of effectors from apoplastic bacteria via kinases (38). We coexpressed NRC4-mKok with GFP fusions of either the closely related helper NLR, NRC2, or the model CC-NLR, ZAR1 and performed live-cell imaging during infection. NRC2-GFP formed unusual filaments throughout the cell, some of which associated with the EHM but did not focally accumulate (Fig. 1O and SI Appendix, Fig. S1). Likewise, ZAR1 did not accumulate around the haustorium but rather showed diffuse cytoplasmic distribution in haustoriated cells much like the GFP control (Fig. 1P and SI Appendix, Fig. S1). Similarly, *N. benthamiana* ZAR1 (NbZAR1) also did not accumulate around haustoria but instead remained peripheral in the cytoplasm and the PM (SI Appendix, Fig. S2A and B). These results demonstrate that not all NLRs accumulate at the haustorium interface like NRC4 and that NRC4 must have unique features or interactors governing haustorium targeting.

NRC4 Localizes to EHM Microdomain(s). The haustorium interface consists of several closely positioned compartments, namely, the plant cytoplasm, the EHM, and the extrahaustorial matrix (12). To determine which haustorial interface compartment NRC4 localizes to, we coexpressed NRC4 with various established marker proteins: cytoplasm marker EV-GFP (SI Appendix, Fig. S3A), EHM markers Remorin1.3 (RFP-Rem1.3) (SI Appendix, Fig. S3B and C) and RPW8.2-BFP (SI Appendix, Fig. S3C), endoplasmic reticulum (ER) marker SP-RFP-HDEL (SI Appendix, Fig. S3D), EHM and peripheral ER marker Synaptotagmin 1 (GFP-SYT1) (SI Appendix, Fig. S3E), and Sucrose transporter 4 (StSUC4-GFP) (SI Appendix, Fig. S3F). We analyzed their localizations and found that NRC4 displays an uneven localization pattern across the EHM and is enriched in certain EHM microdomain(s) (SI Appendix, Supplementary Text) (SI Appendix, Figs. S3 and S4).

N-Terminal $\alpha 1$ Helix of NRC4 Does Not Determine Focal Accumulation to the EHM. Accumulation of NRC4 but not closely related helper NLR NRC2 or the more distantly related MADA-containing NLR ZAR1 at the pathogen interface prompted us to study what part(s) of NRC4's structure is required for EHM trafficking. To determine this, we first investigated the N terminus of NRC4 as the $\alpha 1$ of ZAR1 that covers the MADA motif was reported to facilitate membrane association and act as a death switch (22). We swapped NRC4's $\alpha 1$ onto ZAR1 to see if ZAR1 could gain NRC4's focal accumulation. However, ZAR1^{NRC4 $\alpha 1$} -GFP remained diffuse throughout the cytoplasm (Fig. 2A) like wild type (WT) ZAR1 (Fig. 1P). Next, we performed the reciprocal swap, incorporating the $\alpha 1$ of ZAR1 to NRC4. Previously, we named this chimera ZAR1_{1–17}-NRC4 (23), hereafter named NRC4^{ZAR1 $\alpha 1$} -GFP (Fig. 2G). This chimera retained NRC4's ability to accumulate at the EHM (Fig. 2B), revealing that the first

alpha helix does not determine NRC4's EHM targeting. We confirmed our previous finding that this chimera was functional for HR and disease resistance (23), this time with Rpi-blb2^{nrc4a/b} plants (Fig. 2C). Given the functionality of the chimeric NRC4, we hypothesized a shared mode of action of the $\alpha 1$ of ZAR1 and NRC4. We therefore built a model of NRC4 function based on ZAR1's (Fig. 2D–F). We suggest that NRC4 remains as a monomer or dimer in its resting state, adopting a closed inactive conformation in which the $\alpha 1$ helix remains unexposed as revealed by ZAR1 cryo-EM structure. Following activation, NRC4 also probably oligomerizes and forms a resistosome, and the $\alpha 1$ helix flips out as in the case of activated ZAR1. Considering that the $\alpha 1$ helix is predicted to be buried in the CC domain (Fig. 2D), this model is in agreement with our finding that the $\alpha 1$ helix does not determine the EHM localization (Fig. 2B). If this model is accurate, $\alpha 1$ would only be accessible for membrane association/protein interaction in the active state, but NRC4 accumulates to the EHM in the absence of a sensor NLR (Fig. 1A), that is, the inactive state.

NRC4 Requires a CC Domain to Accumulate at the EHM. We were able to use the homology model (Fig. 2D–F) to determine precise domain boundaries and secondary structure boundaries of NRC4. We therefore investigated the intramolecular determinants of NRC4's focal accumulation by truncating the N terminus to remove the CC domain of NRC4 (NRC4 Δ CC-GFP; NRC4 Δ 1–148-GFP). NRC4 Δ CC-GFP lost its focal accumulation, but in some instances NRC4 Δ CC-GFP formed puncta in the cytoplasm (SI Appendix, Fig. S5A). We quantified the enrichment of NRC4 Δ CC-GFP at the EHM marker RFP-Rem1.3 versus the cytoplasmic marker EV-BFP, using image analysis (SI Appendix, Supplementary Materials and Methods). This revealed that NRC4 Δ CC-GFP was not enriched at the EHM, unlike the full-length NRC4-GFP, which produced a strong fluorescent signal spiking at the EHM (Fig. 3). This indicated that NRC4 requires the CC domain for accumulation at the EHM. However, expression of NRC4's CC domain alone (4CC hereafter; 1 to 148 aa) fused to GFP did not show EHM accumulation (4CC-GFP), suggesting that the CC domain is necessary but not sufficient enough for haustorium targeting of NRC4 (Fig. 3 and SI Appendix, Fig. S5B). This finding also hinted that NRC4 carries additional features governing haustorium trafficking. We next swapped NRC4's CC domain for NRC2's and ZAR1's. Both NRC4^{2CC}-GFP and NRC4^{Z1CC}-GFP still accumulated at the EHM to some degree (Fig. 3 and SI Appendix, Fig. S5C–D), suggesting NRC4 requires a CC domain but not necessarily its own. However, both NRC4^{2CC}-GFP and NRC4^{Z1CC}-GFP appear partially impaired in their EHM accumulation capacities (Fig. 3).

Next, to see if NRC4's CC domain could confer EHM targeting to ZAR1 or NRC2, we generated chimeras of these NLRs containing the CC domain of NRC4. A ZAR1-GFP construct carrying NRC4's CC domain (ZAR1^{4CC}-GFP) did not accumulate at the EHM (Fig. 3 and SI Appendix, S5E). In contrast, introduction of NRC4's CC domain to the more closely related helper NLR NRC2 resulted in gain of function regarding EHM accumulation, as the NRC2^{4CC}-GFP chimera displayed a clear EHM enrichment profile (Fig. 3 and SI Appendix, Fig. S5F). This was an unexpected outcome given the results that NRC4's CC domain alone cannot mediate haustorium enrichment when fused to GFP (4CC-GFP) or introduced into ZAR1 (ZAR1^{4CC}-GFP) backbone. However, these results further support our view that NRCs could carry additional structural features that mediate potential interactions with regulatory components for membrane trafficking.

We next investigated whether any specific region within 4CC could mediate EHM accumulation when introduced into NRC2. 4CC and 2CC share 44% sequence identity and 63% similarity (SI Appendix, Fig. S6). Structural prediction revealed that 4CC encodes four α -helices. The first half of 4CC comprises $\alpha 1$ to 3 helices (aa 1 to 83), and the second half of 4CC (aa 84 to 148)

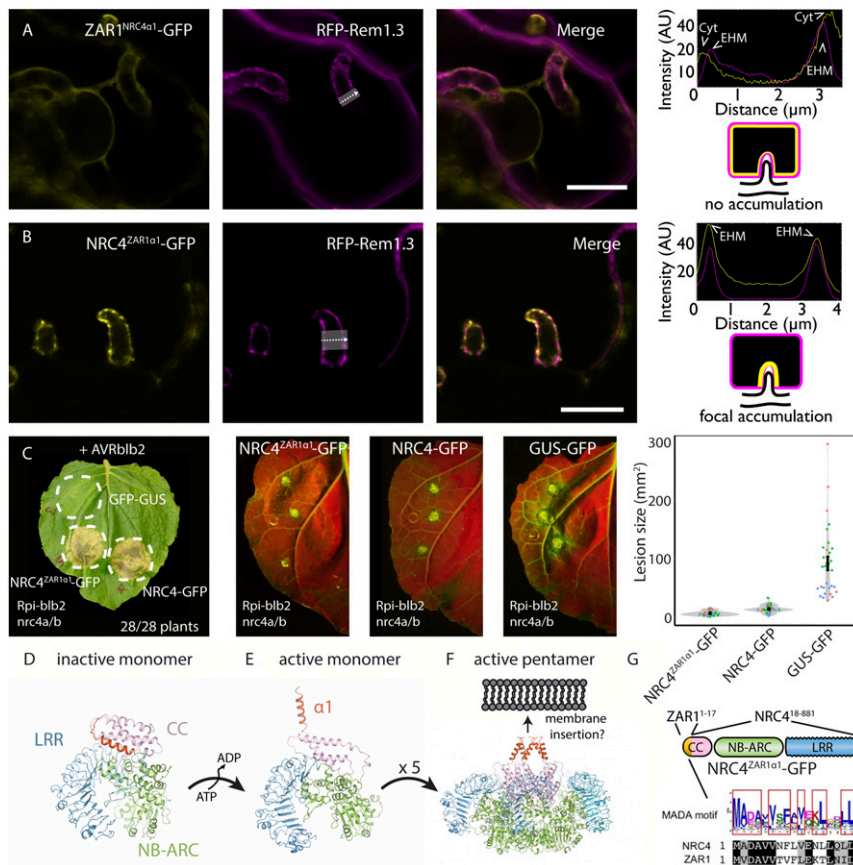


Fig. 2. The first alpha helix of ZAR1 is functional in NRC4 and does not alter its localization. (A) Single-plane confocal image showing ZAR1^{NRC4α1}-GFP does not focally accumulate at EHM but is cytoplasmically localized. (B) Single-plane confocal image showing NRC4^{ZAR1α1}-GFP focally accumulates at EHM with RFP-Rem1.3. (C) NRC4^{ZAR1α1}-GFP and NRC4-GFP but not EV-GFP genetically complements Rpi-blb2^{nrc4a/b} background by triggering HR when coexpressed with AVRblb2 and resistance when expressed alone and infected 1 dpi. The HR assay was repeated with the same results in 28 plants over two independent experiments. Images were taken at 8 dpi. Scattered points in scatter violin plot represent the area (mm²) occupied by infection spots measured on white light images and averaged per leaf, where each construct had $n > 29$ plants/leaves. The mean and SE are shown as points and bars, respectively. Three independent biological replicates were conducted as indicated by color of dots. Ultraviolet (shown) and white light imaging was taken at 8 dpi. Unpaired Wilcoxon tests gave P values of 3.0×10^{-11} for NRC4^{ZAR1α1}-GFP to GUS-GFP, 1.6×10^{-11} for NRC4-GFP to GUS-GFP, and 6.3×10^{-6} for NRC4-GFP to NRC4^{ZAR1α1}-GFP. (D–F) Homology model of NRC4 based on ZAR1 in the (D) inactive ADP-bound state (possibly monomeric), (E) newly active ADP-bound state (possibly monomeric), and (F) where five copies of NRC4 oligomerize into a pentameric resistosome and the five $\alpha 1$ -helices insert into the membrane. CC domain (pink) consists of region 1 to 140 aa, 141 to 157 is a disordered linker region, NB-ARC domain (green) 158 to 495 aa, and LRR (blue) 496 to 843 aa. (G) Model showing location of swap for NRC4^{ZAR1α1}-GFP chimera from A.

comprises $\alpha 4$ and a long, disordered region. We first made intradomain swaps of approximately half of 4CC onto NRC2 backbone (*SI Appendix, Fig. S6*). NRC2^{4CC $\alpha 4$} -GFP gained NRC4's focal accumulation at the EHM (Fig. 3 and *SI Appendix, Fig. S5G*), whereas NRC4^{2CC $\alpha 1-3$} -GFP did not (Fig. 3 and *SI Appendix, Fig. S5H*). Although these findings implicate NRC4's $\alpha 4$ helix in EHM enrichment, this data may seem counterintuitive given the EHM accumulation of NRC4 chimera carrying the CC domain of NRC2 still retains some EHM accumulation capacity (Fig. 3 and *SI Appendix, Fig. S5C*). However, since NRC2 is able to associate with the EHM to an extent (Fig. 10 and *SI Appendix, Fig. S5I*), but does not accumulate (Fig. 3), it is plausible that in addition to the CC domain NRCs foster multiple signatures that determine PM versus EHM localization. The balance between the activities of these different regions could determine subsequent membrane positioning of NRCs during infection.

Activated NRC4 Forms Membrane-Associated Puncta. We next set out to determine the fate of activated NRC4 in infected cells and compare it to the clear EHM accumulation of inactivated NRC4. To do this, we needed to use an NRC4 mutant, which can be

activated but is unable to trigger cell death. Considering the first alpha helix of NRC4 is not involved in EHM targeting, we reasoned we could mutate this region to suppress HR without compromising NRC4's ability to traffic to the EHM. The L9E mutant is predicted to interfere with $\alpha 1$'s ability to insert in the membrane and thus prevent HR (22, 23). Previously, we showed that NRC4^{L9E} mutation suppresses HR and does not provide Rpi-blb2-mediated resistance during transient coexpression with Rpi-blb2 (23). We confirmed these observations in Rpi-blb2^{nrc4a/b} plants (Fig. 4A) and also found that the L9E mutation did not compromise NRC4's ability to traffic to the EHM (Fig. 4B and C).

Considering this mutant is functional in terms of its localization (Fig. 4B), we hypothesized that the L9E mutation renders the NLR defective in triggering HR but is otherwise functional. To simplify the study of NRC4's active and inactive states, we first investigated it in the absence of *P. infestans* infection. When in its inactive, resting state, NRC4^{L9E}-GFP localized to the cytoplasm in Rpi-blb2^{nrc4a/b} plants (Fig. 5A). We next investigated the fate of NRC4^{L9E}-GFP in its activated state, in the presence of an effector. To do this, we coexpressed it with AVRblb2 $\Delta 8$, a truncate of the AVRblb2 that has lost its virulence function but can still trigger HR

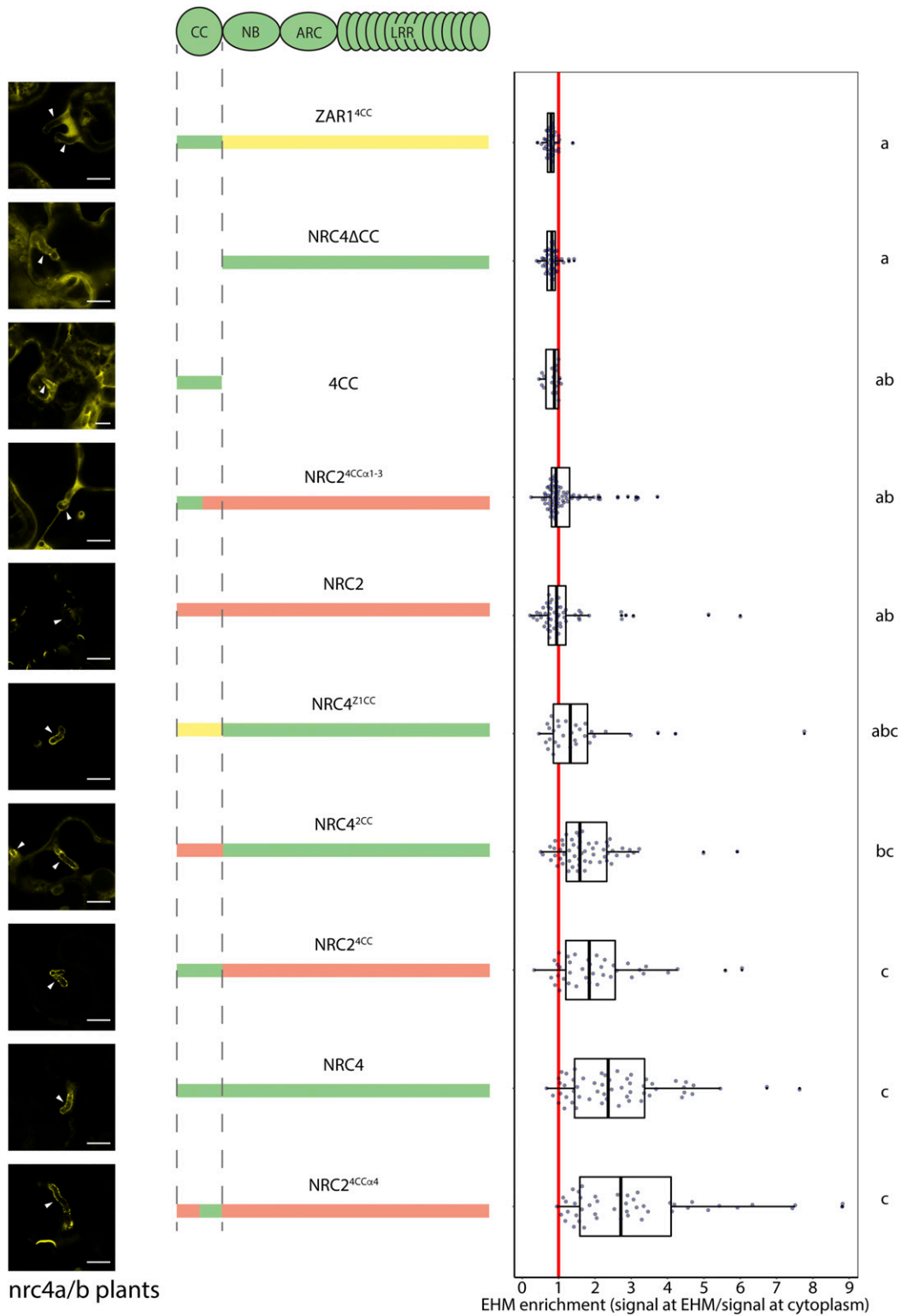


Fig. 3. NRC4 requires a CC domain to accumulate to the EHM. NRC4, NRC2, and ZAR1 C-terminally fused GFP chimeras or truncates were coexpressed with PM and EHM marker RFP-Rem1.3, cytoplasmic marker BFP-EV, and silencing suppressor P19 to boost expression (with the exception of 4CC-GFP, which showed very strong expression). Leaves were infected and after 3 d were imaged with a Leica SP8 microscope. Single-plane micrographs were captured with the names of the constructs blinded to reduce acquisition bias; the image names were also randomized to reduce bias during quantification. A custom ImageJ/FIJI macro was made (see *Materials and Methods*), which allowed us to quantify the GFP signal at the peak RFP position (EHM) and divide it by the GFP signal at the peak BFP position. This is the EHM enrichment, and a number of 1 is no enrichment, and a number of more than 1 is enrichment at the EHM. BFP and RFP channels are available in *SI Appendix, Fig. S5*. Cartoon of chimeric swaps uses green to indicate NRC4, orange to indicate NRC2, and yellow to indicate ZAR1. Each dot on the scatter boxplot corresponds to a single measurement from one haustorium. Significance groupings on the *Right* were determined by first averaging the within-plant values (technical replicates) and then performing an unpaired *t* test.

(14). In the presence of BFP-AVRblb2 Δ 8, activated NRC4^{L9E}-GFP predominantly localized to puncta, which frequently associated with the PM marked by RFP-Rem1.3 (Fig. 5B).

As an alternative to effector activation of NRC4, we used an “autoactive mutant” of NRC4 by adding the D478V MHD mutation to the L9E HR suppressor mutant, in cis (NRC4^{L9E/D478V}). In NRC4^{L9E/D478V}, D478V renders NRC4 autoactive, but the L9E suppresses the cell death (23). We found that NRC4^{L9E/D478V}-GFP localized to puncta in areas of the cell labeled by the membrane marker alone and areas of the cell where the cytoplasmic marker and membrane marker were present (Fig. 5D and E). To validate these observations, we performed membrane enrichment experiments in non-denaturing conditions, followed by sodium dodecyl sulfate–polyacrylamide gel electrophoresis (SDS-PAGE) (Fig. 5F). We found that NRC4^{L9E} was present mostly in the soluble fraction, whereas NRC4^{L9E/D478V} was preferentially found in the membrane-enriched fraction. Lower protein levels of NRC4^{L9E/D478V} overall could be due to increased degradation of active NLRs as reported for RPM1 (32, 39). These biochemical findings, that autoactive NRC4 associates more with membranes, are in agreement with our microscopy that active NRC4 forms puncta, which are mostly associated with the PM. It is possible that these punctate structures represent the oligomerized state of activated NRC4. However, it is unclear whether these are indeed NRC4 resistosomes or perhaps groups of resistosomes enriched in membrane microdomains, and further research is needed to clarify their nature.

To investigate further whether these puncta could constitute resistosomes, we used coimmunoprecipitation of differentially tagged active and inactive NRC4 to ask whether there is an increase in self-association upon activation of NRC4. This has been successfully applied for other NLRs as a means of investigating self-association (40–42). We transiently expressed NRC4^{L9E}-GFP with NRC4^{L9E}-RFP or EV-RFP and NRC4^{L9E/DV}-GFP with

NRC4^{L9E/DV}-RFP or EV-RFP in *nrc4a/b* plants. We then pulled down RFP-tagged proteins and detected RFP and GFP coimmunoprecipitates. We found that autoactive NRC4 self-associated to a higher degree than nonactivated NRC4 (Fig. 5G), which is consistent with oligomerization and resistosome formation.

Activated NRC4 Forms Puncta That Associate with Both the EHM and PM. Next, we investigated the subcellular dynamics of NRC4 when it is activated via the sensor NLR Rpi-blb2 upon recognition of AVRblb2, presumably secreted during *P. infestans* infection. To overcome HR cell death that could limit live-cell imaging, we expressed NRC4^{L9E} mutant in Rpi-blb2^{nrc4a/b} plants or *nrc4a/b* control plants that do not express Rpi-blb2. Remarkably, NRC4^{L9E}-GFP accumulated around haustoria both in Rpi-blb2^{nrc4a/b} and control plants (Fig. 6). However, in the presence of Rpi-blb2, NRC4^{L9E}-GFP formed punctate structures across the EHM (Fig. 6A and B and *SI Appendix, Fig. S7A*). Additionally, in haustoriated Rpi-blb2^{nrc4a/b} plants, NRC4^{L9E}-GFP often displayed clear labeling of the PM and puncta that are located at the PM (Fig. 6A and *SI Appendix, Fig. S7A* and *Movie S4*). In other cases, NRC4^{L9E}-GFP did not accumulate at the EHM in Rpi-blb2^{nrc4a/b} plants, but instead there was equal labeling of the EHM and PM, and puncta localized at both the EHM and PM (*SI Appendix, Fig. S7B*). We quantified the PM enrichment of NRC4^{L9E}-GFP in cells penetrated by haustoria in *nrc4a/b* plants versus Rpi-blb2^{nrc4a/b} plants. We found a significant increase in PM enrichment in the presence of the sensor NLR Rpi-blb2 (*SI Appendix, Fig. S7C*). These results reveal that activated NRC4 does not exclusively accumulate at the haustorium, showing PM localization to an extent, and forms puncta that mainly remain associated with the EHM but also localize at the PM. Remarkably, autoactive NRC4^{L9E/D478V}-GFP did not accumulate at the EHM at all but instead produced fluorescent signal scattered throughout the infected cell similar to the EV-GFP control

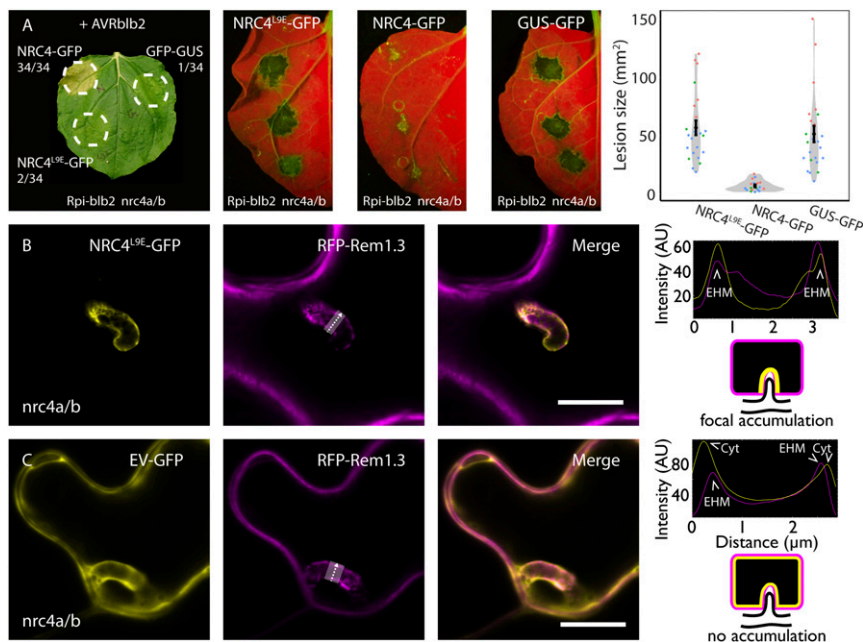


Fig. 4. NRC4^{L9E} is nonfunctional for HR and *P. infestans* resistance but still focally accumulates at the EHM. (A) NRC4-GFP, but not NRC4^{L9E} mutant or EV-GFP, genetically complements CRISPR/Cas mutation of Rpi-blb2^{nrc4a/b} plants by triggering HR when coexpressed with AVRblb2 and resistance when expressed alone and infected 1 dpi. The HR assay was repeated with the same results in 34 plants over two independent experiments. Images were taken at 3 dpi. Scattered points in scatter violin plot represent the area (mm²) occupied by infection spots measured on white light images, where each construct had $n > 17$ plants/leaves. Three independent experimental replicates were conducted as indicated by color of dots. Ultraviolet (representative images for three constructs) and white light imaging was taken at 8 dpi. Wilcoxon unpaired tests gave P values of 5.8×10^{-8} for NRC4^{L9E}-GFP to NRC4-GFP, 0.28 for NRC4^{L9E}-GFP to GUS-GFP, and 7.6×10^{-8} for NRC4-GFP to GUS-GFP. (B and C) Single-plane confocal micrographs showing NRC4^{L9E}-GFP focally accumulates at EHM with RFP-Rem1.3 but not the EV-GFP control, which remains cytoplasmic. (Scale bars, 10 μ m.)

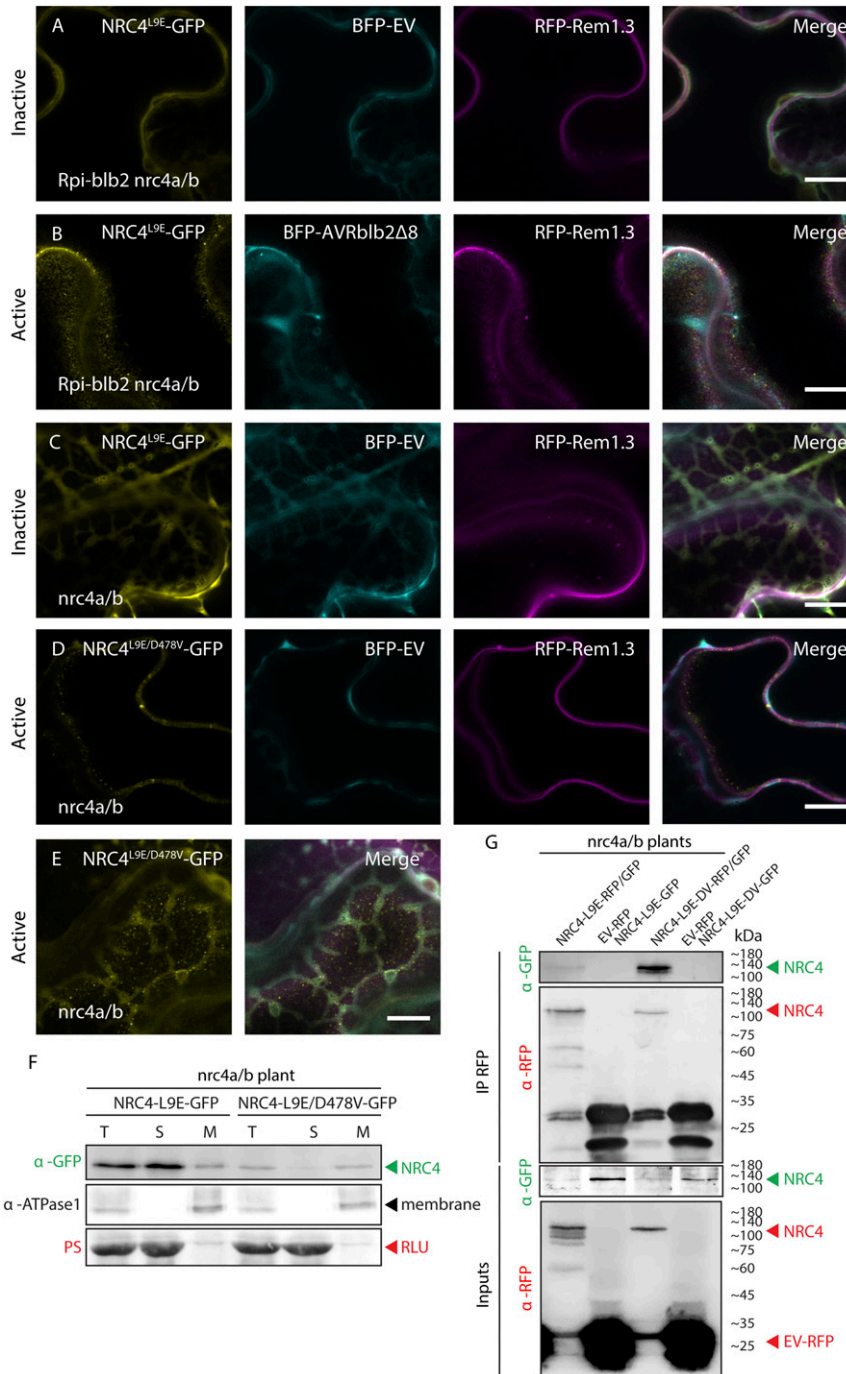


Fig. 5. Activated NRC4 forms puncta associated with the PM in the absence of *P. infestans* infection. (A–E) Single-plane confocal micrographs showing the localization of active and inactive variants of NRC4, with PM marker RFP-Rem1.3 and cytoplasmic BFP marker. (Scale bars, 10 μ m.) (A) NRC4^{L9E}-GFP is localized to the cytoplasm in *Rpi-blb2^{nrc4a/b}* plants when coexpressed with BFP-EV. (B) NRC4^{L9E}-GFP forms puncta associated with the PM when coexpressed with effector protein truncate BFP-AVRblb2Δ8. (C) NRC4^{L9E}-GFP is localized to the cytoplasm when coexpressed with BFP-EV and RFP-Rem in *nrc4a/b* plants. (D and E) Autoactive NRC4^{L9E/D478V}-GFP forms puncta associated with the PM and patches of the cell labeled by both the cytoplasmic marker and membrane marker. (F) Membrane enrichment confirms inactive NRC4^{L9E}-GFP is mostly localized to the soluble (cytoplasmic) fraction, whereas autoactive NRC4^{L9E/D478V}-GFP is more associated with the membrane fraction. T = total, S = soluble, M = membrane, PS = ponceau stain, RLU = rubisco large subunit. (Top) Green arrowhead indicates expected band sizes of GFP-tagged NRC4 proteins. (Middle) Black arrowhead indicates expected band size of ATPase1 membrane marker. (G) Coimmunoprecipitation experiment showing autoactive NRC4 self-associates more than inactive NRC4. NRC4^{L9E}-GFP transiently coexpressed with NRC4^{L9E}-RFP or EV-RFP control was compared with NRC4^{L9E/DV}-GFP transiently coexpressed with NRC4^{L9E/DV}-RFP or EV-RFP control. *N. benthamiana* leaf tissue was frozen 3 dpi, and RFP-tagged proteins were immunoprecipitated with RFP-trap agarose beads and immunoprecipitates (IP-RFP), and total protein extracts (Input) were immunoblotted with appropriate antibodies. Arrowheads indicate expected band sizes of proteins labeled.

(Fig. 6 C and D). However, unlike GFP control, NRC4^{L9E/D478V}-GFP mainly labeled the PM and frequently produced puncta that were mostly associated with the PM but also with the EHM to some degree (Fig. 6 C and D), indicating that activated NRC4 could redefine its membrane targeting route.

Based on these findings, we propose a model (EHM release model—Fig. 6E) in which the nonactivated NRC4 accumulates at the haustorium interface, positioning itself at effector delivery sites, possibly to improve its activation potential and to accelerate the deployment of the immune response. While activated

NRC4 forms puncta associated with the EHM, some of the activated NRC4 is released from this initial site of activation to target the PM, possibly to propagate immune signaling and enhance the HR cell death response. Activated NRC4 could potentially form oligomers as illustrated by activated ZAR1 model, forming resistosomes that target the EHM and PM (Fig. 6E).

Discussion

Here, we identified an immune mechanism in which an NLR undergoes dynamic changes in its subcellular localization during

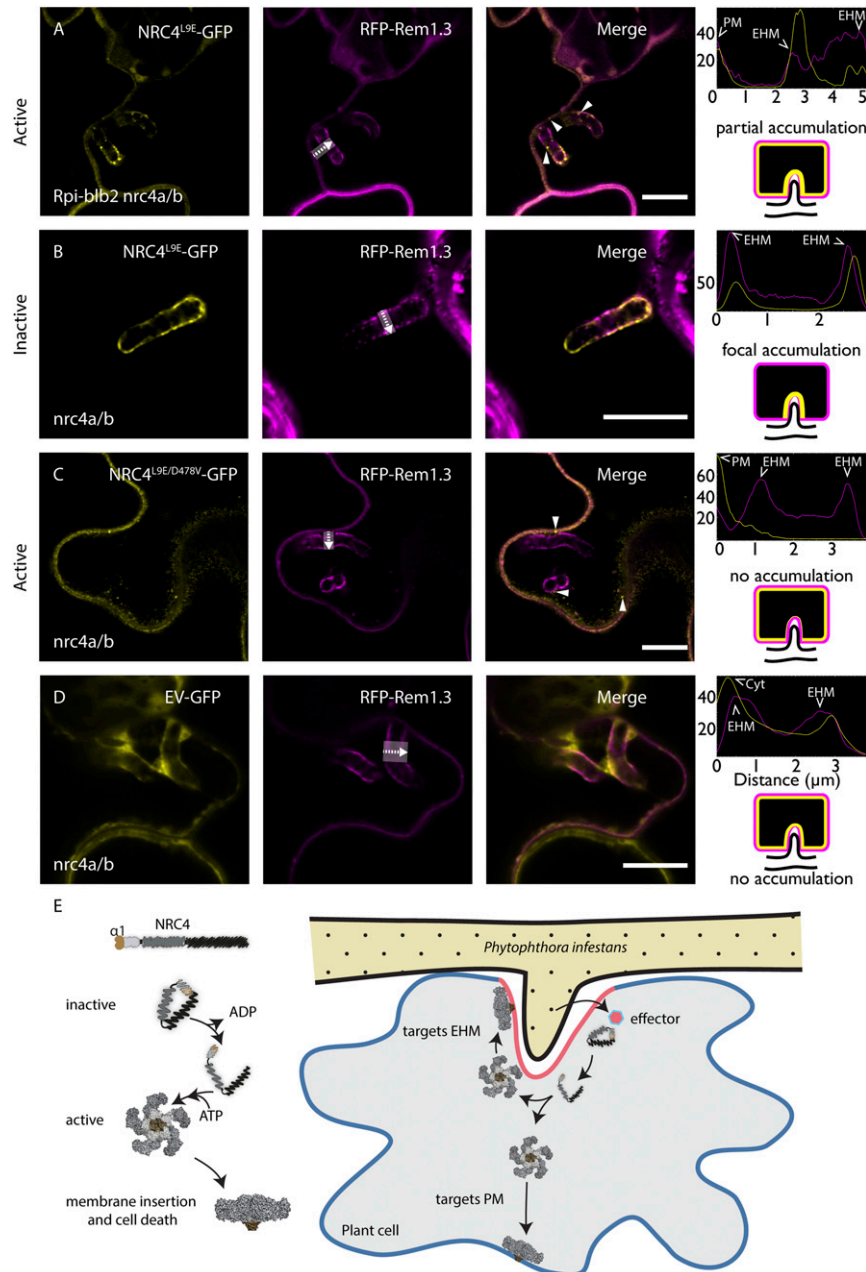


Fig. 6. NRC4 is activated by Rpi-blb2 during infection and forms puncta that associate with the EHM and PM. (A–D) Single-plane confocal micrographs showing the localization of active and inactive variants of NRC4, with PM marker RFP-Rem1.3 during infection with *P. infestans*. (Scale bars, 10 μ m.) (A) NRC4^{L9E}-GFP forms puncta associated with the EHM and PM in Rpi-blb2^{nrc4a/b} plants and partially but not fully accumulates at the EHM. (B) NRC4^{L9E}-GFP focally accumulates to the EHM in nrc4a/b plants. (C) NRC4^{L9E/D478V}-GFP does not focally accumulate at the EHM but instead forms puncta on the PM and EHM in nrc4a/b plants. (D) EV-GFP does not focally accumulate or form puncta in nrc4a/b plants. (E) Model depicting possible modes of action of NRC4 where NRC4 gets activated via sensor NLRs (not shown) at the EHM by detecting periaustorial effectors. NRC4 then oligomerizes into a resistosome and targets the EHM, but a population of resistosomes dissociates from the EHM to target the PM. These resistosomes insert into the membrane to cause programmed cell death.

infection, positioning itself at the specialized plant–pathogen interface where the corresponding pathogen effectors are deployed. Strikingly, following immune recognition, the activated NLR further reorganizes to form punctate structures not only at the pathogen interface membrane but also at the distant PM, suggesting that activated NLRs could possibly propagate from the primary site of activation to distant membrane interfaces. We report that NLRs are not necessarily stationary immune receptors during infection but instead can have inactive and active states shuttling to and from effector delivery sites.

Whether there is immune signaling at the EHM is currently unknown. In this work, we uncovered that the inactive form of the helper NLR, NRC4, accumulates at the EHM surrounding the *P. infestans* haustorium. Considering the prominent roles of the EHM in facilitating effector translocation and nutrient uptake by the pathogen, as well as secretion of plant defense compounds, it is not surprising that the pathogen deploys effectors to this site or that the plant deploys NLRs guarding it. Conceivably, positioning of receptors where their ligands accumulate would enhance their chances of recognition. In fact, several receptors have been found to colocalize with their cognate effectors or reposition themselves (32–36, 43, 44), though this has not been shown during infection with relevant microbes. Consistent with the view that NLRs would reposition to detect effectors, two *P. infestans* effectors that accumulate at the haustorium interface, AVRblb2 and AVR1, are recognized by NRC4-dependent sensor NLRs Rpi-blb2 and R1, respectively (13, 14, 21). Intriguingly, both AVRblb2 and AVR1 are implicated in interfering with defense-related secretion (13, 14, 16). AVRblb2 interferes with secretion of an immune protease via an unknown mechanism, whereas AVR1 targets a key member of the secretory pathway, Sec5 of the exocyst complex at the EHM (13, 16). Therefore, we speculate that NRC4 could be guarding components of vesicle trafficking and fusion at the EHM by pairing with various sensor NLRs to monitor potential manipulation by effectors.

These findings implicate NLRs in plant focal immune responses. *P. infestans* is a useful model for studying focal immunity because of the large haustorial interface, which allows clear identification of focal responses due to the substantial changes that occur upon haustorium penetration. However, focal immunity is not just restricted to haustoria-forming pathogens (45–49). Therefore, our findings could also be relevant to nonhaustoria-forming pathogens and pests such as bacteria, nematodes, insects, and viruses. Consistent with this view, NRC4 also pairs with sensor NLRs that recognize nematodes, insects, bacteria, and viruses (21). Each has an interface with the host, which could be targeted by plant focal immunity, and it would be interesting to determine if NLRs are repositioned in these pathosystems. Another aspect not investigated here is the possible role(s) of NRC4 in immunity independent of other sensor NLRs, that is, in wild-type plants, for instance via surface immune receptors. However, we noticed that NRC4 still accumulated to the EHM in BAK1 silenced plants (*SI Appendix, Fig. S8*), indicating BAK1 may not be required for NRC4's focal accumulation at the EHM.

Here, we discovered that NRC4 but not closely related helper NLR NRC2 or the distantly related MADA NLR ZAR1 accumulates at the EHM (Fig. 1 *O* and *P*). Intriguingly, NRC2 formed fibril-like structures or filaments some of which associate with the EHM, but overall, it did not show accumulation like NRC4 (Fig. 10 and *SI Appendix, Fig. S44*). Whether other NLRs accumulate at the EHM remains to be determined. The atypical plant resistance protein RPW8.2, which lacks NB or LRR domains, was shown to localize to the EHM (50). However, how it contributes to immunity is still unknown. Some NLRs contain an RPW8-like N-terminal domain instead of a CC or TIR domain. These CC_R's include ADR1 and NRG1, which are now known to be helper NLRs for multiple TNLs and CC-NLRs (51–53). In addition, ADR1 and NRG1 are known to be required for resistance to several haustoria-forming pathogens (51,

53). Whether these helper NLRs also target the EHM would be interesting to determine. It could be that focal accumulation of NLRs to the EHM is a common resistance mechanism against haustoria-forming oomycetes and fungi.

Considering our finding that NRC2 and ZAR1 do not focally accumulate at the EHM (Fig. 1 *O* and *P*), it draws into question how NRC4 achieves this feat. We found that NRC4 relies on a CC domain to enable focal accumulation at the haustorium interface but that its CC domain alone is not enough for this process (Fig. 3 and *SI Appendix, Fig. S5 A and B*). However, NRC2 gained focal accumulation from transfer of NRC4's CC domain or even the second half of the CC domain (Fig. 3 and *SI Appendix, Fig. S5 F–G*). This indicates that the $\alpha 4$ and/or the disordered region at the end of the CC domain contains one signature that determines focal accumulation. However, it's likely another signature is required for focal accumulation and that this is found in NRCs but not all NLRs, as ZAR1 did not gain focal accumulation upon transfer of NRC4's CC domain (Fig. 3 and *SI Appendix, Fig. S5E*). The requirement for an EHM-targeting signature found in the NB domain or an LRR domain fits our hypothesis that NRC4 does not traffic to the EHM via the same pathway as RPW8.2, bearing in mind that RPW8.2 does not require an NB or LRR domain for EHM localization. The EHM-targeting signatures of NRC4 may be structural or sequence specific and involve intermolecular associations with trafficking pathways targeted to the EHM.

Intriguingly, we found that not only the preactivated NRC4 but also the activated NRC4 shifts its localization pattern in response to infection. During infection of plants that carry the sensor NLR Rpi-blb2, we noticed perturbations in NRC4 accumulation at the EHM (Fig. 6*A* and *SI Appendix, Fig. S7 A and B*), as we noticed additional NRC4-GFP signal at the PM. We recapitulated these findings using an autoactive mutant form of NRC4, which did not exclusively accumulate at the EHM but instead mainly labeled the PM (Fig. 6*C*). We also confirmed, with membrane enrichment experiments, that NRC4 can increase its association with membranes upon activation (Fig. 5*F*). These results revealed that activated NRC4 does not accumulate at the EHM, possibly because it could undergo conformational changes upon activation, leading to its dissociation from the EHM. Autoactive NRC4 may change such that it is unable to accumulate at the EHM or no longer prefers the EHM, unlike the inactive form. Alternatively, autoactive NRC4 may simply target the nearest membrane. The MADA CC-NLR ZAR1 undergoes a large conformational change, whereby it assembles into a pentameric resistosome, which subsequently targets the PM to create pores and trigger cell death (22, 23, 27). Whether ZAR1 mode of action could be applied to other MADA CC-NLRs still remains to be addressed. However, our previous and current work suggest that NRC4 mediated HR cell death, and resistance can be maintained in NRC4 chimeras carrying the N-terminal $\alpha 1$ region of ZAR1 that was indicated to make membrane pores (Fig. 2*C*) (23, 27).

We discovered that activated NRC4-GFP forms distinct puncta that associate with the PM in uninfected cells (Fig. 5 *B, D*, and *E*). In agreement with our model of activation then EHM release, activation of NRC4 via a sensor NLR during infection also leads to formation of NRC4 puncta that associate with the EHM and PM (Fig. 6*A* and *SI Appendix, Fig. S7 A and B*). These NRC4 puncta could emerge at and remain associated with the EHM following effector recognition, whereas some could be released from this primary site of activation to target the PM throughout the cell. Alternatively, activated NRC4 monomers could also disassociate from the EHM, get enriched at the PM, and form puncta there, possibly to propagate immune responses throughout the cell and enhance the HR. Such repositioning of an NLR protein has also been reported following activation of the mammalian NLRP3 receptor. Prior to its activation, NLRP3 remains in the ER and cytosol, whereas activated NLRP3 assembles into inflammasome targeting various organelles, presumably to

enhance perception of danger signals and enhance inflammasome assembly (54).

But what are these NRC4 puncta? One plausible explanation is that these are oligomers of NRC4 that assemble into resistosome like ZAR1. In fact, this is consistent with our observation that autoactive NRC4 self-associates more than the nonactive form of NRC4 (Fig. 5G). Whether the puncta presented here represent resistosomes or clusters of resistosomes remains to be determined. However, two recent papers have shown that activated NLRs form puncta that associate with the PM, and these puncta are associated with pore formation and calcium influx, leading to cell death (27, 55). These data would indicate that the active-NLR associated puncta are resistosomes or at least groups of resistosomes. If validated, this method for identifying resistosomes by expressing HR-suppressed variants by mutation of their MADA motif, coupled with live-cell confocal microscopy, can be a quick and easy way to monitor resistosome formation, instead of challenging techniques such as Blue-Native PAGE, which is also not truly *in vivo*.

Here, we introduced a cell biology dimension to study NLR function during live-cell infection. So far, this has not been feasible due to cell suicide following NLR activation. We have established methods and tools to overcome this limitation (NRC mutant plants and point mutants that prevent HR but not trafficking) to employ live-cell infection imaging of NLRs in haustoriated cells. Particularly, by investigating the trafficking of NRC4, a helper NLR that accumulates at the haustorium interface in a unique fashion, we provide insights into the dynamics of NLR activation in infected cells. Dissecting the functional

principles of plant NLRs and their cellular dynamics during infection are not only critical basic mechanistic studies but also will guide future studies to design synthetic NLRs that can boost immune activation at the pathogen interface.

Materials and Methods

All experiments were conducted with *N. benthamiana* and, excluding those experiments stated using transgenic plants, were conducted with Agrobacterium-mediated transient gene expression. Microscopy during infection or "infection assays" were done by collecting zoospores in cold water from wild-type or tdTomato 88069 *P. infestans* grown on rye sucrose agar and infecting with 10- μ L drops containing ~700 spores on the abaxial or adaxial side of the leaf depending on experiments. Confocal microscopy was carried out with Leica SP8 or SP5 resonance microscope. Molecular cloning was carried out with a combination of high-fidelity PCR, gene synthesis, Gibson assembly, and Golden-gate assembly. Further details can be found in *SI Appendix, Supplementary Materials and Methods*.

Data Availability. All study data are included in the article and/or supporting information.

ACKNOWLEDGMENTS. We thank Dr. Sebastian Schornack, Dr. Khaoula Belhaj, and Dr. Yasin Dagdas for the great comments and suggestions over the years. We thank Dr. Joe Win for sending materials and for the discussions. We thank the following funding agencies: Imperial Schrödinger PhD Scholarship (C.D.), Research England UK GCRF (C.D.), BBSRC (Grant BB/T006102/1) (C.D.), BBSRC DTP (E.M., Z.S., and A.Y.L.), and Gatsby Charitable Foundation (H.A., C.-H.W., A.M., and S.K.). The Facility for Imaging by Light Microscopy (S.M.R.) at Imperial College London is partly supported by funding from the Wellcome Trust (Grant 104931/Z/14/Z) and BBSRC (Grant BB/L015129/1).

1. S. Wang *et al.*, Delivery of cytoplasmic and apoplastic effectors from *Phytophthora infestans* haustoria by distinct secretion pathways. *New Phytol.* **216**, 205–215 (2017).
2. S. Wang *et al.*, The *Phytophthora infestans* haustorium is a site for secretion of diverse classes of infection-associated proteins. *mBio* **9**, 1–14 (2018).
3. E. Kemen *et al.*, Identification of a protein from rust fungi transferred from haustoria into infected plant cells. *Mol. Plant Microbe Interact.* **18**, 1130–1139 (2005).
4. R. T. Voegelé, C. Struck, M. Hahn, K. Mendgen, The role of haustoria in sugar supply during infection of broad bean by the rust fungus *Uromyces fabae*. *Proc. Natl. Acad. Sci. U.S.A.* **98**, 8133–8138 (2001).
5. K. Mendgen, P. Nass, The activity of powdery-mildew haustoria after feeding the host cells with different sugars, as measured with a potentiometric cyanine dye. *Planta* **174**, 283–288 (1988).
6. S. C. Whisson *et al.*, A translocation signal for delivery of oomycete effector proteins into host plant cells. *Nature* **450**, 115–118 (2007).
7. T. O. Bozkurt *et al.*, The plant membrane-associated REMORIN1.3 accumulates in discrete periaustorial domains and enhances susceptibility to *Phytophthora infestans*. *Plant Physiol.* **165**, 1005–1018 (2014).
8. T. O. Bozkurt *et al.*, Retargeting of plant late endocytic trafficking toward a pathogen interface. *Traffic* **16**, 204–226 (2015).
9. S. Koh, A. André, H. Edwards, D. Ehrhardt, S. Somerville, *Arabidopsis thaliana* subcellular responses to compatible *Erysiphe cichoracearum* infections. *Plant J.* **44**, 516–529 (2005).
10. Y.-J. Lu *et al.*, Patterns of plant subcellular responses to successful oomycete infections reveal differences in host cell reprogramming and endocytic trafficking. *Cell. Microbiol.* **14**, 682–697 (2012).
11. C. O. Micali, U. Neumann, D. Grunewald, R. Panstruga, R. O'Connell, Biogenesis of a specialized plant-fungal interface during host cell internalization of Golovinomyces orontii haustoria. *Cell. Microbiol.* **13**, 210–226 (2011).
12. T. O. Bozkurt, S. Kamoun, The plant-pathogen haustorial interface at a glance. *J. Cell Sci.* **133**, jcs237958 (2020).
13. S. Wang *et al.*, *Phytophthora infestans* RXLR effectors act in concert at diverse subcellular localisations to enhance host colonisation. *J. Exp. Bot.* **70**, 343–356 (2018).
14. T. O. Bozkurt *et al.*, *Phytophthora infestans* effector AVRblb2 prevents secretion of a plant immune protease at the haustorial interface. *Proc. Natl. Acad. Sci. U.S.A.* **108**, 20832–20837 (2011).
15. D. G. O. Saunders *et al.*, Host protein BSL1 associates with *Phytophthora infestans* RXLR effector AVR2 and the *Solanum demissum* Immune receptor R2 to mediate disease resistance. *Plant Cell* **24**, 3420–3434 (2012).
16. Y. Du, M. H. Mpina, P. R. J. Birch, K. Bouwmeester, F. Govers, *Phytophthora infestans* RXLR effector AVR1 interacts with exocyst component Sec5 to manipulate plant immunity. *Plant Physiol.* **169**, 1975–1990 (2015).
17. R. F. Oliva *et al.*, A recent expansion of the RXLR effector gene Avrblb2 is maintained in global populations of *Phytophthora infestans* indicating different contributions to virulence. *Mol. Plant Microbe Interact.* **28**, 901–912 (2015).
18. S.-K. Oh *et al.*, In planta expression screens of *Phytophthora infestans* RXLR effectors reveal diverse phenotypes, including activation of the *Solanum bulbocastanum* disease resistance protein Rpi-blb2. *Plant Cell* **21**, 2928–2947 (2009).
19. E. A. G. van der Vossen *et al.*, The Rpi-blb2 gene from *Solanum bulbocastanum* is an Mi-1 gene homolog conferring broad-spectrum late blight resistance in potato. *Plant J.* **44**, 208–222 (2009).
20. Y. Du *et al.*, RXLR effector diversity in *Phytophthora infestans* isolates determines recognition by potato resistance proteins; the case study AVR1 and R1. *Stud. Mycol.* **89**, 85–93 (2018).
21. C. H. Wu *et al.*, NLR network mediates immunity to diverse plant pathogens. *Proc. Natl. Acad. Sci. U.S.A.* **114**, 8113–8118 (2017).
22. J. Wang, *et al.*, Reconstitution and structure of a plant NLR resistosome conferring immunity. *Science* **364**, eaav5870 (2019).
23. H. Adachi *et al.*, An N-terminal motif in NLR immune receptors is functionally conserved across distantly related plant species. *eLife* **8**, 693291 (2019).
24. M. Hu, J. Qi, G. Bi, J.-M. Zhou, Bacterial effectors induce oligomerization of immune receptor ZAR1 *in vivo*. *Mol. Plant* **13**, 793–801 (2020).
25. J. Wang, *et al.*, Ligand-triggered allosteric ADP release primes a plant NLR complex. *Science* **364**, eaav5868 (2019).
26. H. Burdett *et al.*, The plant "resistosome": Structural insights into immune signaling. *Cell Host Microbe* **26**, 193–201 (2019).
27. G. Bi *et al.*, The ZAR1 resistosome is a calcium-permeable channel triggering plant immune signaling. *Cell* **184**, 3528–3541.e12 (2021).
28. Q. H. Shen, P. Schulze-Lefert, Rumble in the nuclear jungle: Compartmentalization, trafficking, and nuclear action of plant immune receptors. *EMBO J.* **26**, 4293–4301 (2007).
29. Y.-H. Chiang, G. Coaker, Effector triggered immunity: NLR immune perception and downstream defense responses. *Arab. B.* **13**, e0183 (2015).
30. D. Qi, R. W. Innes, Recent advances in plant NLR structure, function, localization, and signaling. *Front. Immunol.* **4**, 348 (2013).
31. F. El Kasmi *et al.*, Signaling from the plasma-membrane localized plant immune receptor RPM1 requires self-association of the full-length protein. *Proc. Natl. Acad. Sci. U.S.A.* **114**, E7385–E7394 (2017).
32. Z. Gao, E.-H. Chung, T. K. Eitas, J. L. Dangl, Plant intracellular innate immune receptor Resistance to *Pseudomonas syringae* pv. *maculicola* 1 (RPM1) is activated at, and functions on, the plasma membrane. *Proc. Natl. Acad. Sci. U.S.A.* **108**, 7619–7624 (2011).
33. D. Qi, B. J. DeYoung, R. W. Innes, Structure-function analysis of the coiled-coil and leucine-rich repeat domains of the RPS5 disease resistance protein. *Plant Physiol.* **158**, 1819–1832 (2012).
34. J. L. Caplan, P. Mamillapalli, T. M. Burch-Smith, K. Czymmek, S. P. Dinesh-Kumar, Chloroplastic protein NR1P1 mediates innate immune receptor recognition of a viral effector. *Cell* **132**, 449–462 (2008).
35. Q. H. Shen, *et al.*, Nuclear activity of MLA immune receptors links isolate-specific and basal disease-resistance responses. *Science* **315**, 1098–1103 (2007).

36. S. Engelhardt *et al.*, Relocalization of late blight resistance protein R3a to endosomal compartments is associated with effector recognition and required for the immune response. *Plant Cell* **24**, 5142–5158 (2012).
37. J. Wang, *et al.*, Reconstitution and structure of a plant NLR resistosome conferring immunity. *Science* **364**, 1–36 (2019).
38. D. Seto *et al.*, Expanded type III effector recognition by the ZAR1 NLR protein using ZED1-related kinases. *Nat. Plants* **3**, 17027 (2017).
39. D. C. Boyes, J. Nam, J. L. Dangl, The *Arabidopsis thaliana* RPM1 disease resistance gene product is a peripheral plasma membrane protein that is degraded coincident with the hypersensitive response. *Proc. Natl. Acad. Sci. U.S.A.* **95**, 15849–15854 (1998).
40. T. Qi *et al.*, NRG1 functions downstream of EDS1 to regulate TIR-NLR-mediated plant immunity in *Nicotiana benthamiana*. *Proc. Natl. Acad. Sci. U.S.A.* **115**, E10979–E10987 (2018).
41. S. C. Saile *et al.*, Coiled-coil and RPW8-type immune receptors function at the plasma membrane in a 2 phospholipid dependent manner. *bioRxiv* [Preprint] (2020). <https://doi.org/10.1101/2020.11.18.388520>. Accessed 20 February 2021.
42. Z. Wu *et al.*, TIR signaling promotes the interactions between EDS1/PAD4 and ADR1-L1 and oligomerization of ADR1-L1. *bioRxiv* [Preprint] (2021). <https://doi.org/10.1101/2021.05.23.445317>. Accessed 27 May 2021.
43. L. Wirthmueller, Y. Zhang, J. D. G. Jones, J. E. Parker, Nuclear accumulation of the *Arabidopsis* immune receptor RPS4 is necessary for triggering EDS1-dependent defense. *Curr. Biol.* **17**, 2023–2029 (2007).
44. Y. T. Cheng *et al.*, Nuclear pore complex component MOS7/Nup88 is required for innate immunity and nuclear accumulation of defense regulators in *Arabidopsis*. *Plant Cell* **21**, 2503–2516 (2009).
45. C. S. Bestwick, I. R. Brown, J. W. Mansfield, Localized changes in peroxidase activity accompany hydrogen peroxide generation during the development of a nonhost hypersensitive reaction in lettuce. *Plant Physiol.* **118**, 1067–1078 (1998).
46. C. S. Bestwick, I. R. Brown, M. H. R. Bennett, J. W. Mansfield, Localization of hydrogen peroxide accumulation during the hypersensitive reaction of lettuce cells to *Pseudomonas syringae* pv phaseolicola. *Plant Cell* **9**, 209–221 (1997).
47. C. S. Bestwick, M. H. Bennett, J. W. Mansfield, Hrp mutant of *Pseudomonas syringae* pv phaseolicola induces cell wall alterations but not membrane damage leading to the hypersensitive reaction in lettuce. *Plant Physiol.* **108**, 503–516 (1995).
48. E. Schmelzer, Cell polarization, a crucial process in fungal defence. *Trends Plant Sci.* **7**, 411–415 (2002).
49. C. Kwon, P. Bednarek, P. Schulze-Lefert, Secretory pathways in plant immune responses. *Plant Physiol.* **147**, 1575–1583 (2008).
50. W. Wang, Y. Wen, R. Berkey, S. Xiao, Specific targeting of the *Arabidopsis* resistance protein RPW8.2 to the interfacial membrane encasing the fungal haustorium renders broad-spectrum resistance to powdery mildew. *Plant Cell* **21**, 2898–2913 (2009).
51. L. M. Jubic, S. Saile, O. J. Furzer, F. El Kasm, J. L. Dangl, Help wanted: Helper NLRs and plant immune responses. *Curr. Opin. Plant Biol.* **50**, 82–94 (2019).
52. D. Lapin *et al.*, A coevolved EDS1-SAG101-NRG1 module mediates cell death signaling by TIR-domain immune receptors. *Plant Cell* **31**, 2430–2455 (2019).
53. B. Castel *et al.*, Diverse NLR immune receptors activate defence via the RPW8-NLR NRG1. *New Phytol.* **222**, 966–980 (2019).
54. C. Hamilton, P. K. Anand, Right place, right time: Localisation and assembly of the NLRP3 inflammasome. *FT000 Res.* **8**, 1–12 (2019).
55. P. Jacob, *et al.*, Plant “helper” immune receptors are Ca²⁺-permeable nonselective cation channels. *Science* **7917**, eabg7917 (2021).